Low-Temperature NMR Studies of Zn Tautomerism and Hindered Rotations in Solid Zincocene Derivatives

Juan Miguel Lopez del Amo,[†] Gerd Buntkowsky,[‡] Hans-Heinrich Limbach,*[,†] Irene Resa,[§] Rafael Fernández,[§] and Ernesto Carmona[§]

Institut für Chemie und Biochemie der Freien Universität Berlin, Takustrasse 3, D-14195, Berlin, Germany, Institut für Physikalische Chemie, Friedrich-Schiller Universität, Jena, Helmholtzweg 4, D 07743 Jena, Germany, and Instituto de Investigaciones Químicas, CSIC, Avda. Américo Vespucio 49, 41092 Sevilla, Spain

Received: December 6, 2007; In Final Form: February 6, 2008

Using a combination of NMR methods we have detected and studied fluxional motions in the slip-sandwich structure of solid decamethylzincocene (**I**, [(η^5-C_5Me_5)Zn(η^1-C_5Me_5)]). For comparison, we have also studied the solid iminoacyl derivative [(η^5-C_5Me_5)Zn(η^1-C(NXyl)C_5Me_5)] (**II**). The variable temperature ^{13}C CPMAS NMR spectra of **I** indicate fast rotations of both Cp* rings in the molecule down to 156 K as well as the presence of an order−disorder phase transition around 210 K. The disorder is shown to be dynamic arising from a fast combined Zn tautomerism and η^1/η^5 reorganization of the Cp* rings between two degenerate states A and B related by a molecular inversion. In the ordered phase, the degeneracy of A and B is lifted; that is, the two rings X and Y are inequivalent, where X exhibits a larger fraction of time in the η^5 state than Y. However, the interconversion is still fast and characterized by a reaction enthalpy of $\Delta H = 2.4$ kJ mol^{-1} and a reaction entropy of $\Delta S = 4.9$ J K^{-1} mol^{-1}. In order to obtain quantitative kinetic information, variable temperature ^{2}H NMR experiments were performed on static samples of **I**-d_6 and **II**-d_6 between 300 and 100 K, where in each ring one CH_3 is replaced by one CD_3 group. For **II**-d_6, the ^{2}H NMR line shapes indicate fast CD_3 group rotations and a fast "η^5 rotation", corresponding to 72° rotational jumps of the η^5 coordinated Cp* ring. The latter motion becomes slow around 130 K. By line shape analysis, an activation energy of the η^5 rotation of about 21 kJ mol^{-1} was obtained. ^{2}H NMR line shapes analysis of **I**-d_6 indicates fast CD_3 group rotations at all temperatures. Moreover, between 100 and 150 K, a transition from the slow to the fast exchange regime is observed for the 5-fold rotational jumps of both Cp* rings, exhibiting an activation energy of 18 kJ mol^{-1}. This value was corroborated by ^{2}H NMR relaxometry from which additionally the activation energies 6.3 kJ mol^{-1} and 11.2 kJ mol^{-1} for the CD_3 rotation and the molecular inversion process were determined.

Introduction

Metallocenes constitute one of the most important families of organometallic compounds.[1] Their general structure corresponds to MCp′$_2$, where M represents a metal and Cp′ represents any cyclo-pentadienyl-type ligand. Metallocenes are endowed with a distinguished history, and moreover, they enjoy multiple applications in different areas of chemistry, such as polymerization catalysis, asymmetric catalysis (e.g., chiral ferrocenyl ligands), bio-organometallic chemistry, and others.[1] The metallocene era started in 1951 with the preparation of Fe(C_5H_5)$_2$[2] and with the recognition by Fischer and Wilkinson et al. of its correct, now well-known, π-bonded sandwich structure.[3] In 1959, Fischer and co-workers reported the preparation of Be(C_5H_5)$_2$[4a] and Zn(C_5H_5)$_2$,[4b] but it was only in the following decades, with the development of the substituted bulky cyclopentadienyl ligands,[1,5] that the similarity between beryllocenes and zincocenes became apparent. In contrast to the divalent metallocenes of the transition elements that feature invariably a sandwich structure, the analogous metallocenes of the main group elements exhibit a variety of structures that include types **1**−**5**, schematically depicted in Scheme 1.[6] To our knowledge

SCHEME 1: Molecular Structures of Metallocenes

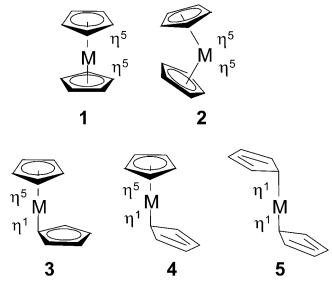

a structure of type **4** was proposed only for the B(C_5Me_5)$_2^{2+}$ cation[7] and more recently for Zn(η^5-$C_5Me_4SiMe_3$)(η^1-C_5Me_4-$SiMe_3$).[8] Most beryllocenes[9] and zincocenes[10] exhibit geometries of type **3**, the so-called slipped-sandwich structure, also referred to as $\eta^5/\eta^1(\pi)$. This peculiar structure is characterized by nearly parallel Cp′ rings, by a relatively weak and long M−C bond to the η^1 ring and by extensive π-electron delocalization within the latter. The question then arises whether the $\eta^1(\pi)$ binding is closer to the η^5 or to the η^1 binding type. Unfortunately, it is not easy to study this question experimentally.

Some of us have reported recently the synthesis and structural characteristics of the methyl-substituted beryllocenes Be(C_5Me_5)$_2$, Be(C_5Me_4H)$_2$, and Be(C_5Me_5)(C_5Me_4H).[9a] With the only exception of Be(C_5Me_5)$_2$, which in the solid-state exhibits an

* Corresponding author. E-mail: juanmi@chemie.fu-berlin.de.
[†] Freie Universität Berlin.
[‡] Friedrich Schiller Universität Jena.
[§] CSIC Sevilla.

10.1021/jp711504g CCC: $40.75
Published on Web 03/27/2008

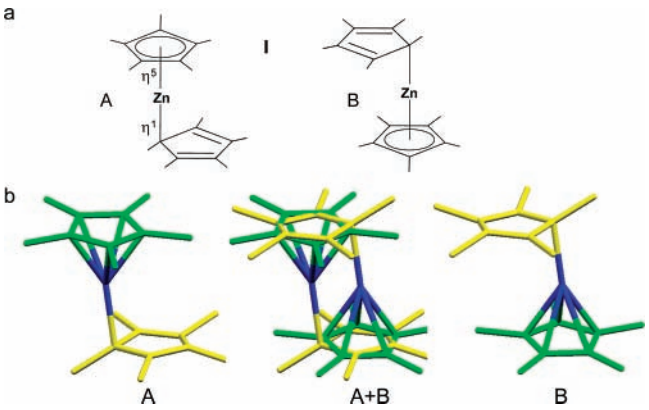

Figure 1. (a) Schematic representation of the decamethylzincocene molecule (**I**) in the forms A and B related by inversion symmetry. (b) Stick representation of the X-ray structure of **I**. Forms A and B are shown separately, as well as superimposed (A + B). This last form corresponds to the actual unit cell observed in the X-ray structure.

almost regular sandwich geometry, possibly as a consequence of crystal packing effects, they feature $\eta^5/\eta^1(\pi)$ coordination of the Cp′ rings. The compounds are fluxional, both in solution and in the solid-state, as the slipped-sandwich structure is characterized by a flat potential energy surface. Ab initio calculations show that the latter contains several minima exhibiting only small energy differences, associated with isomeric η^5/η^1 structures which interconvert via a η^5/η^5 structure.[9a] Indeed, for the parent beryllocene, $Be(C_5H_5)_2$, two dynamic processes involving very low activation energies had been identified by MD calculations at 400 K.[11] They consisted of a 1,5-sigmatropic shift of the (η^5-C_5H_5)Be unit around the periphery of the η^1 ring, involving an η^5/η^2 transition state (E_a = 5 kJ mol^{-1}), and of a ring-exchange process, or molecular inversion, that interchanges the roles of the two rings from η^5 to η^1 and vice versa (E_a = 8 kJ mol^{-1}). The latter was proposed to occur through an η^3/η^3 transition state.[11] During the course of our work, the dynamics of the known beryllocenes have been investigated by solid-state ^{13}C and ^{9}Be NMR spectroscopy.[12] Unfortunately, the dynamic range of this method is limited.

As we were interested in studying the solid-state dynamics of this unusual slipped-sandwich metallocene structure, particularly the effect of an $\eta^5/\eta^1(\pi)$ interaction on the activation energies, we concentrated our efforts on decamethylzincocene ($Zn(C_5Me_5)_2$, **I**) in order to avoid the high toxicity of beryllium and its compounds. **I** was prepared in 1986 by the reaction of NaC_5Me_5 and $ZnCl_2$ and characterized by gas electron diffraction as (η^5-C_5Me_5)Zn(η^1-C_5Me_5).[10c] Subsequent X-ray studies led also to this geometry for the monomeric molecules of Zn-($C_5Me_5)_2$, with the zinc atom disordered between two equivalent sites (Figure 1). In the unit cell, two equivalent molecules A and B are superimposed (A + B). Both molecules together exhibit an inversion center. As such slip-sandwich geometries are associated with highly fluxional structures,[9,11] we expected the following dynamic processes.

The first process, the "molecular inversion" or ring-exchange process, is illustrated in Figure 2a. It does not consist of a real 180° rotation of the whole molecule in the unit cell as one might infer from this figure. However, it is the result of a displacement of the central Zn ion between two positions in the unit cell. This displacement is coupled to the following geometrical changes of each of the Cp* rings, (i) anticooperative twist jumps of both rings by approximately 10° and (ii) a simultaneous reorganization of the skeleton of each ring from a planar disposition in the η^5 form to a nonplanar in the η^1 or vice-

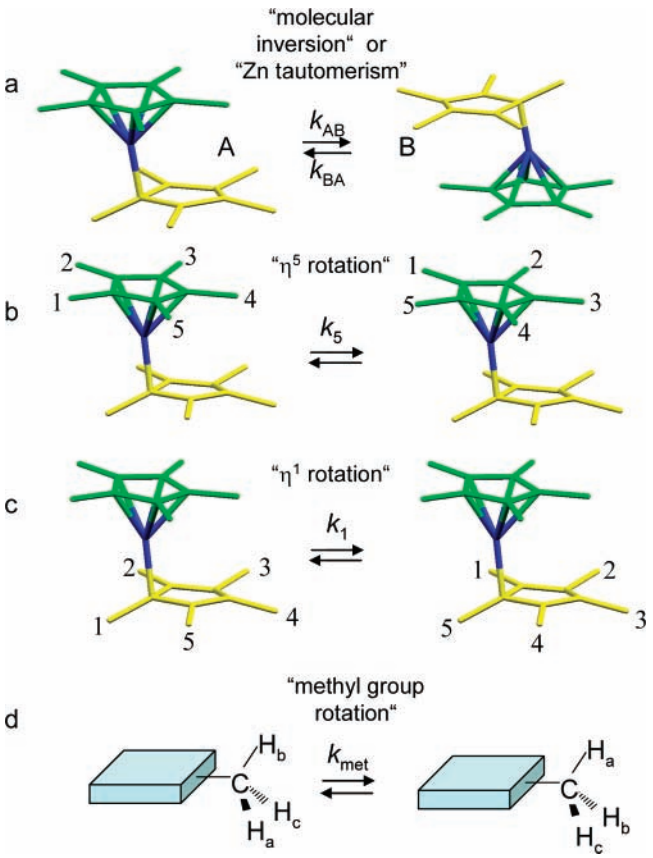

Figure 2. Fluxional motions observed in **I**. (a) The molecular inversion process or Zn tautomerism: interchange the role of both ring η^5 (green) and ring η^1(yellow) by the Zn tautomerism (blue) between the two equivalent positions. The overall result is equivalent to an inversion of the molecule. In (b) and (c), the η^5 and η^1 rotation processes are shown. (d) Methyl group rotation corresponding to 120° jumps.

versa, due to the partial σ character of the Zn-(η^1)Cp* bond. In other words, the process consists of a Zn displacement coupled to an interchange of the "hapticity" of both rings. The overall result of this motion is equivalent to a molecular inversion. However, as this term corresponds to a symmetry operation and not to a real molecular rearrangement, we prefer to call the process "Zn tautomerism". The process presumably involves an $\eta^3-\eta^3$ intermediate.

The second process consists of internal ring rotations, that is, an interconversion of the carbon atoms and methyl groups in each ring. The "η^5 rotation" (Figure 2b) consists of rotational 72° jumps around the ring axis. This internal rotation leaves the sequence of bonds unchanged. The "η^1 rotation" (Figure 2c) of the η^1 bound ring also consists of rotational jumps, however, coupled to a reorganization of the skeleton. It is also known as "1,5-sigmatropic shift".

Finally, the fastest intramolecular process one can expect is methyl group rotations which interchange the three equivalent proton atoms by rotation around the C−C bond as illustrated in Figure 2d.

Because of the limited dynamic range of solid state ^{13}C NMR, we thought that solid state ^{2}H NMR line shape analyses and relaxometry of suitably deuterated decamethylzincocene should provide much more kinetic information about the above-mentioned processes. Therefore, we introduced a deuterated methyl group into each Cp* of **I** as a molecular probe. For comparison, we have also prepared the iminoacyl complex (η^5-C_5Me_5)Zn(η^1-C(NXyl)C_5Me_5) (**II**) (see Figure 3; Xyl = 2,6-$Me_2C_6H_2$) containing only one η^5 ring as well as the analog

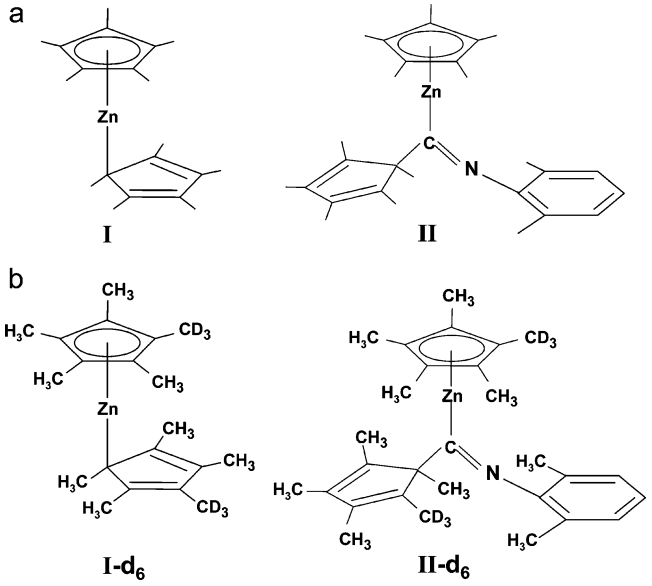

Figure 3. (a) Chemical structures of compounds **I** and **II**. (b) Left: structure of **I**-d_6 used for the ^{2}H NMR experiments. Right: deuterated sample used for the ^{2}H NMR solid state measurements of the iminoacyl [(η^5-C_5Me_5)Zn(C(NXyl)C_5Me_5)]. Each ring contains a single CD_3 group. Each methyl group position can accommodate the CD_3 group; however, only a single isotopolog is depicted for each compound.

complex containing a CD_3 group in each ring for ^{2}H NMR measurements. The interest in **II** arises from the fact that it is only subject to methyl group rotations and to the "η^5 rotation", whereas the Zn tautomerism and the η^1 rotation are suppressed. Thus, **II** was very useful to confirm the analyses of the dynamic NMR experiments performed on **I**.

This paper is organized as follows. After a theoretical section dealing with the relation between NMR spectra and the different molecular motions illustrated in Figure 2 and an experimental section, we describe the results of our NMR experiments on **I** and **II**. The latter are then analyzed and discussed.

Theoretical Section

In this section, we discuss how the processes listed in Figure 2 can influence the line shapes of the ^{13}C signals of **I** measured under the conditions of magic angle spinning (MAS), cross polarization (CP), and ^{1}H decoupling.

For a given molecule of **I**, the Zn tautomerism depicted in Figure 2a which takes place between two forms A and B is not necessarily a degenerate process. Therefore, it may be characterized by the equilibrium constant

$$K_{AB} = k_{AB}/k_{BA} = x_B/x_A = \exp(\Delta S_{AB}/R - \Delta H_{AB}/RT) \qquad (1)$$

Here, ΔH_{AB} and ΔS_{AB} represent the reaction enthalpy and reaction entropy, R is the gas constant, k_{AB} and k_{BA} are the forward and backward rate constants, and x_A and x_B are the corresponding mole fractions.

Generally, exchange broadened NMR line shapes are described in terms of the quantum-mechanical density matrix formalism proposed by Binsch et al.[13] Using this theory, various NMR line shapes of heavy atom nuclei in the presence of nondegenerate exchange reactions have been calculated.[14] As illustrated at the top of Figure 4, let us denote the upper ring as "X" and the lower ring as "Y". Figure 4a shows the calculated separate line shape contributions of X and of Y to the high resolution ^{13}C spectrum when the rate constant k_{AB} is increased. In the slow exchange regime, X exhibits in form A the intrinsic

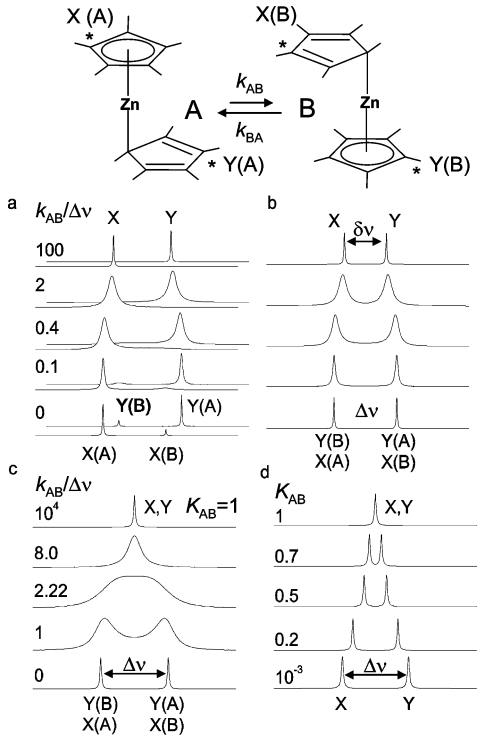

Figure 4. (a) ^{13}C NMR subspectra and (b) spectra calculated for different rate constants k_{AB} of the nondegenerate Zn transfer exhibiting an equilibrium constant of $K_{AB} \neq 1$. (c) Calculated spectra for a degenerate Zn transfer with $K_{AB} = 1$. (d) Calculated spectra for a nondegenerate fast Zn transfer as a function of K_{AB}.

chemical shift $\nu_X(A)$ while Y exhibits the chemical shift $\nu_Y(A)$. Similarly, $\nu_X(B)$ and $\nu_Y(B)$ represent the intrinsic shifts of form B. Let us assume a very reasonable assumption for the ^{13}C nuclei of **I** that

$$\nu_X(A) = \nu_Y(B) \qquad \nu_X(B) = \nu_Y(A)$$
$$\text{i.e. } \Delta\nu = \nu_X(A) - \nu_X(B) \quad (2)$$

Let us also assume that A dominates, that is, that $K_{AB} < 1$. Neglecting any anisotropic nuclear interactions, we obtain for both rings the usual features of a nondegenerate exchange process as depicted in Figure 4a. The sum of the two contributions gives the total line shape depicted in Figure 4b. Thus, only two lines are observed in the slow exchange regime, which broaden and coalesce into two new lines. The latter exhibit a reduced splitting $\delta\nu = \nu_X - \nu_Y$ from which the equilibrium constant can be calculated[14]

$$K_{AB} = (1 - \delta\nu/\Delta\nu)/(1 + \delta\nu/\Delta\nu) \qquad (3)$$

In Figure 4c, we have considered the degenerate case with $K_{AB} = 1$, which shows the usual features. In Figure 4d, we have considered the case of very fast exchange, where the value of the equilibrium constant K_{AB} varies from a very small value to a value of 1. Here, the two lines continually shift toward each other and can be obtained from the splitting K_{AB} according to eq 3 if $\Delta\nu$ is known from low-temperature spectra.

We note that if the intrinsic line widths are large, it is sometimes not easy to distinguish the cases of Figure 4c,d.

Experimental Section

Synthesis of I and II and Their d_6 Isotopomers. All preparations and manipulations were carried out under oxygen-free argon using conventional Schlenk techniques. Solvents were

rigorously dried and degassed before use. Infrared spectra were recorded on a Bruker Vector 22 spectrometer. NMR spectra were recorded on Bruker DRX-500 spectrometers. The ^{1}H, ^{2}H, and ^{13}C resonances of the solvent were used as the internal standard, and the chemical shifts are reported relative to TMS.

1,2,3,4,5-Pentamethylcyclopentadiene-*d*$_3$. This ligand was prepared by the literature procedure reported for C_5Me_5H.[15] 2,3,4,5-tetramethylcyclopenten-2-enone (2.22 g, 2.4 mL, 15.29 mmol) was added to a solution of $CD_3Li\cdot LiI$ (36 mL, 18 mmol, 0.5 M Et_2O). The remaining methyl lithium was hydrolyzed with methanol (1 mL) and water (1 mL), and the mixture was washed with a solution prepared with ammonium chloride (0.24 g), concentrated hydrochloric acid (0.2 mL), and water (0.1 mL). The aqueous phase was extracted with ether (25 mL), and the organic layers were stirred for 30 min with 1 mL of HCl, then washed twice with 50 mL of 5% $NaHCO_3$ solution, and finally dried over K_2CO_3 to yield 1.86 g (13.38 mmol, 87%) of the product. ^{1}H NMR (500 MHz, C_6D_6, 20 °C): 0.98 (d, 3H, J = 8 Hz), 1.73 (s, 6H), 1.78 (s, 6H), 2.40 (m, 1H). ^{2}H NMR (500 MHz, C_6H_6, 20 °C): 0.91 (s, 3D), 1.66 (s, 6D), 1.71 (s, 6D). ^{13}C{^{1}H} NMR (125 MHz, C_6D_6, 20 °C): 10.9 (2 Me$_\beta$), 11.4 (2 Me$_\alpha$), 13.9 (Me), 51.28, 51.44, 51.48 (CH; three isotopomers), 134.1 (C$_\beta$), 137.2 (C$_\alpha$).

$KC_5Me_4(CD_3)$. To a suspension of KH (532 mg, 13.26 mmol) in THF (35 mL) was added a solution of $C_5Me_4(CD_3)H$ (1.86 g, 13.38 mmol) in the same solvent (10 mL). The mixture was stirred at room temperature during 36 h, and the solvent was then removed under vacuum. The solid residue was washed twice with 30 mL of hexane and dried in vacuo to yield 2.14 g (12.1 mmol, 90%) of the salt.

$Zn(C_5Me_4CD_3)_2$. This compound was prepared in accordance with the literature procedure[10c] but by using the deuterated salt. A mixture of 205 mg (1.5 mmol) of $ZnCl_2$ and 531 mg (3 mmol) of $KC_5Me_4CD_3$ was stirred in 30 mL of THF, at room temperature, for 1 h. The crude product was extracted with pentane to yield the compound as a white solid that was recrystallized from pentane (320 mg, 0.95 mmol, 65%). ^{1}H NMR (500 MHz, C_6D_6, 25 °C, ppm): 1.87 (Me). ^{2}H NMR (500 MHz, C_6H_6, 25 °C, ppm): 1.81 (CD_3). ^{13}C{^{1}H} NMR (125 MHz, C_6D_6, 25 °C, ppm): 11.2 (C−*Me*), 111.8 (*C*−Me). IR (Nujol, cm^{-1}): 2063 (ν_{CD3}).

(η^5-C_5Me_5)Zn(η^1-C(NXyl)C_5Me_5) (II). $Zn(C_5Me_5)_2$ (746 mg, 2.2 mmol) and CNXyl (288 mg, 2.2 mmol) were dissolved in 50 mL of hexane, and the resulting solution was stirred at room temperature for 5 h. ^{1}H NMR monitoring revealed the reaction was complete. The solvent was then removed under vacuum, the resulting yellow solid was extracted with 30 mL of hexane and crystallized from this solvent. Yield: 840 mg, 1.8 mmol, 82%. ^{1}H NMR (500 MHz, C_6D_6, 25 °C, ppm): 1.70 (s, 15H), 1.46 (s, 3H,), 1.72 (s, 6H), 1.82 (s, 6H), 2.02 (s, 6H), 6.87 (t, 1H, *p*-C*H*-Ar), 7.03 (d, 2H, *m*-C*H*-Ar). ^{13}C{^{1}H} NMR (125 MHz, C_6D_6, 25 °C, ppm): 9.8 (η^5-CH_3), 10.8 (Me), 11.2 (2 *Me*), 14.2 (2 Me), 18.6 (2 *Me*), 70.9 (C_q), 105.7 (*C*H), 107.8 (C_q), 122.5 (C-Me), 128.5 (*C*H), 137.5 (C−Me), 140.0 (C−Me) 156.2 (C_q−N), 198.9 (C═N). IR (nujol, cm^{-1}): 1585 ($\nu_{C=N}$). Elemental analysis calcd (%) for $C_{29}H_{39}NZn$: C 74.62, H 8.35, N 2.99. Found: C 74.6, H 7.7, N 2.9.

Compound **II**-d_6 was prepared as above, starting from **I**-d_6 (320 mg, 0.94 mmol), CNXyl (123 mg, 0.94 mmol), and 30 mL of hexane as the reaction solvent. The yield of the product from the first crop of crystals was 220 mg, approximately 50%. The remaining product was discarded.

Low-Temperature Solid State ^{2}H NMR Measurements. A detailed discussion of our home-built three channel NMR spectrometer has been given recently.[16] Here, only some salient features are reproduced. All experiments were performed at a field of 7 T, corresponding to a ^{2}H resonance frequency of 46.3 MHz on a standard Oxford wide bore magnet (89 mm) equipped with a room-temperature shim unit. For the ^{2}H channel, a 2 kW class AB amplifier from AMT equipped with an RF-blanking for suppressing the noise during data acquisition was employed. The RF was fed through a crossed diode duplexer, connected to the detection preamplifier and through the filters into the probe. Typical ^{2}H pulse width was 5.0 μs, corresponding to 50 kHz B_1 field in frequency units. To achieve a better excitation of the echo spectrum, a shortened pulse with of 3.5 μs was employed.

All experiments were performed using a home-built 5 mm ^{2}H NMR probe. The probe is placed in a dynamic Oxford CF1200 helium flow cryostat. The sample temperature was controlled employing an Oxford ITC 503 temperature controller. During cooling and before and after data acquisition, the sample temperature was directly controlled via a Cernox sensor placed in the direct vicinity of the sample. This temperature was used to calibrate the readings of a second CGR-1-1000 sensor, which is part of the cryostat. During data acquisition, the first sensor was disconnected from the ITC 503 and grounded to protect the ITC from the RF and to avoid distortions of the signal. Because of the high sensitivity of the ^{2}H NMR line shapes of both **I**-d_6 and **II**-d_6 on the temperature, we carefully monitored the stabilization and equilibration of the temperature, allowing stabilization times up to several hours at each temperature before performing the NMR experiment.

All spectra were recorded in resonance using the solid echo technique, with an echo spacing of 30 μs and a full 8-step phase cycle, which removes artifacts from FIDs of the two pulses. Before Fourier transformation, the echo-signal was phase corrected, and the imaginary part was zeroed to give fully symmetric spectra, which are better suited for the line shape analysis.

^{2}H NMR Data Evaluation. The ^{2}H-echo spectra in the fast and slow exchange regime were simulated employing a laboratory written Matlab program. Instead of numerically performing the powder integration, the faster analytical expression of the powder pattern in terms of elliptic integrals[17] was used to calculate the line shape for infinite T_2. The ^{2}H NMR echo spectra of **I**-d_6 in the intermediate exchange regime were simulated by a self-written Matlab routine using a Liouville formalism of the exchange process, described recently.[18]

^{13}C NMR Measurements. All ^{13}C NMR measurements were performed on a Bruker MSL-300 instrument, operating at 7 T, equipped with a Chemagnetics-Varian variable-temperature 6 mm pencil CPMAS probe. The magic angle spinning (MAS, 7000 Hz) NMR experiments were performed employing the {^{1}H}^{13}C CPMAS technique with a cross-polarization contact time of 5 ms. All ^{13}C chemical shift values were referenced to solid adamantane.

Results

Synthesis and Spectroscopic Properties of I and of II. Decamethylzincocene can be readily prepared by the reported procedure[10c] that involves the reaction of anhydrous $ZnCl_2$ with NaC_5Me_5. The potassium salt of the ligand, KC_5Me_5, may alternatively be used, and in either case, $Zn(C_5Me_5)_2$ can be isolated as an air-sensitive white crystalline solid in moderate yields (ca. 60%; we have been unable to reproduce the reported 96% yield).[10c] Low-temperature ^{1}H NMR studies of solutions of this complex revealed[10b] a highly fluxional behavior,

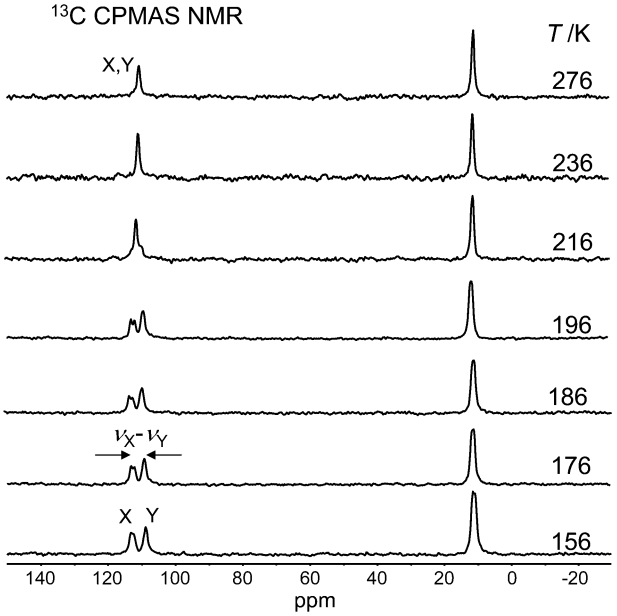

Figure 5. Variable temperature ^{13}C CPMAS NMR spectra of **I** recorded at 75 MHz (7 T).

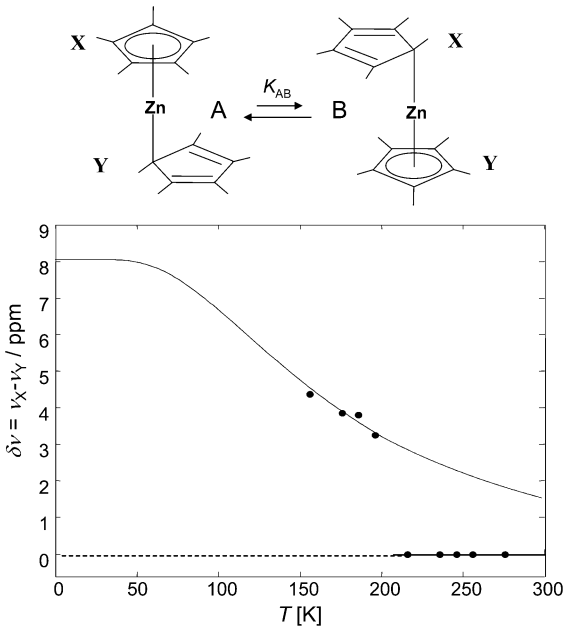

Figure 6. Experimental and predicted ^{13}C chemical shift difference $\delta\nu = \nu_X - \nu_Y$ of the two aromatic rings of **I** (Table 1, Figure 5). Above 216 K, a single line is observed corresponding to a disordered solid with two equivalent rings X and Y, that is, $\delta\nu = 0$. Below 200 K, both rings become inequivalent and $\delta\nu > 0$. The solid line was fitted to the experimental low-temperature data using eq 3.

evinced by the observation of only one methyl signal down to −100 °C. Similarly, only one ^{13}C resonance was detected at 111.6 ppm for the ring quaternary carbons.[10b] In this regard, it is worth mentioning that in half sandwich compounds of the type (η^5-C_5Me_5)ZnR (R = Me, Et) and other related complexes (see below for **II**), the ring carbon nuclei resonate invariably in the very narrow range of 107.5−109 ppm.[19]

Upon adding 1 mol equivalent of CNXyl to solutions of **I** at room temperature, a smooth reaction ensues that yields the iminoacyl **II** as the only reaction product. IR and NMR data for **II** are in agreement with the proposed formulation.

The Zn-η^1-C(NXyl)C_5Me_5 linkage features a distinct IR absorption at 1590 cm^{-1} and a low-field ^{13}C NMR resonance

TABLE 1: ^{13}C NMR Chemical Shifts and Line Separations of the Aromatic Signals of I

T/K	δ_X/ppm	δ_Y/ppm	$\delta_X-\delta_Y$/ppm
276	110.8		0
256	110.8		0
246	111.0		0
236	111.0		0
216	111.0		0
196	112.5	109.2	3.3
186	113.0	109.2	3.8
176	113.0	109.2	3.9
156	113.2	108.9	4.4

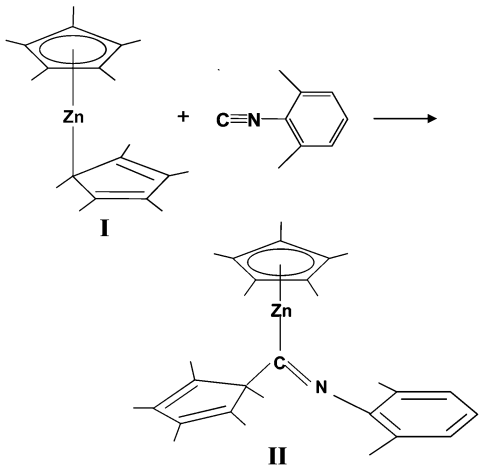

(4)

at 198.9 ppm. These data are comparable to those reported for the analogous beryllium iminoacyl (η^5-C_5Me_5)Be(η^1-C(NXyl)C_5-Me_5).[20] The ring carbon nuclei of the (η^5-C_5Me_5)Zn moiety of **II** give a ^{13}C{^{1}H} NMR signal at δ 107.8, while those of the iminoacyl functionality appear at 139.9, 137.5, and 70.9 ppm. These and other data summarized in the Experimental Section provide unequivocal support for the structure of **II** shown in eq 4, which has been independently confirmed by X-ray crystallography.[21]

Variable Temperature ^{13}C CPMAS NMR of Compounds I and II. The variable temperature ^{13}C CPMAS spectra of compound **I** are shown in Figure 5. The spectra recorded at higher temperatures (276 to 216 K) are characterized by two lines arising from the aromatic (110.8 ppm) and methyl (10.9 ppm) carbons. The presence of common signals for all of the aromatic and methyl groups in the spectra is indicative of degenerate fast ring rotations and fast molecular inversion rates, whose combination gives rise to a situation in which both rings and the different positions inside each ring are indistinguishable by ^{13}C NMR. At lower temperatures (from 216 to 196 K), on the other hand, the aromatic signal suddenly splits into two lines with equal intensities within the margin of error. By further lowering the temperature, the splitting $\delta\nu = \nu_X - \nu_Y$ between these two lines increases gradually. These effects are highlighted in Figure 6. The sudden splitting of the aromatic line below 200 K is characteristic of a phase transition, in which the degeneracy of the Zn tautomerism present at the high temperatures is lost. In this regime, the spectral features correspond to those of Figure 4d and not to those of Figure 4c. All chemical shifts and line separations are summarized in Table 1. In order to calculate the equilibrium constants K_{AB} below 200 K using eq 3 and the solid line in Figure 6, we needed to know the intrinsic chemical shift difference

$$\Delta\nu = \nu_X(A) - \nu_X(B) = \nu_Y(B) - \nu_Y(A) \qquad (5)$$

between the two rings. Unfortunately, we were not able to reach

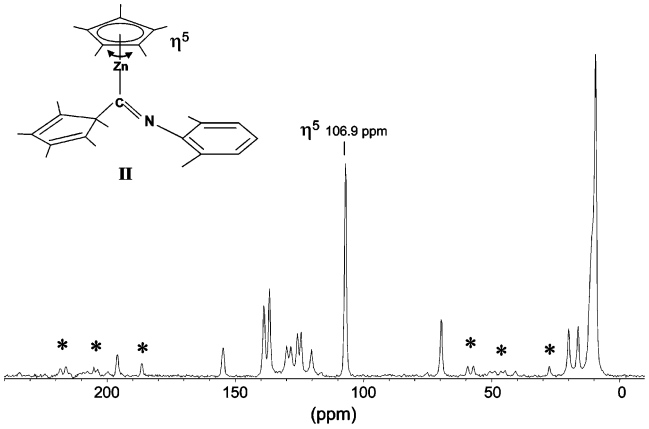

Figure 7. ^{13}C CPMAS NMR spectra of **II**. The signal obtained for the aromatic η^5 carbons (106.9 ppm) is used in order to extract the intrinsic chemical shift values of **I** in the variable temperature spectra of Figure 6, as explained in the text.

the low temperatures required to obtain this value. Therefore, we proceeded as follows. We assumed that all chemical shifts are temperature independent and that the chemical shift of the η^5 bound ring in **I** is the same as the corresponding ring in **II** whose room-temperature ^{13}C CP MAS spectrum is depicted in Figure 7. The spectrum was not analyzed in detail, but the signal of the Cp* ring at 106.9 ppm could be easily identified. Thus, we set

$$\nu_X(\mathrm{A}) \cong \nu(\mathrm{II} - \eta^5) = 106.9 \text{ ppm} \quad (6)$$

As the average high-temperature chemical shift of the aromatic carbons of **I** is given by

$$\nu_{X,Y}(298\mathrm{K}) = 1/2\ (\nu_X(\mathrm{A}) + \nu_X(\mathrm{B})) = 110.8 \text{ ppm} \quad (7)$$

we obtained a chemical shift value of

$$\nu_X(\mathrm{B}) = 114.9 \text{ ppm} \qquad \text{or} \qquad \Delta\nu = 8 \text{ ppm} \quad (8)$$

Keeping now the value of $\Delta\nu$ fixed, we could adapt the calculated solid line in Figure 6 to the experimental data by varying the reaction enthalpy and the reaction entropy. Thus, we obtained the values $\Delta H = 2.4$ kJ/mol and $\Delta S = 4.9$ J/mol K. The temperature dependence of the equilibrium constant can then be expressed as

$$K_{AB} = 1.8 \exp(-289 / T) \qquad \text{for } T \le 200 \text{ K}$$
$$K_{AB} = 1 \qquad \text{for } T \ge 200 \text{ K} \quad (9)$$

Variable Temperature ^{2}H NMR of II-d_6. In Figure 8, the variable temperature ^{2}H NMR spectra of **II**-d_6 are shown. The spectrum at 180 K consists clearly of a superposition of two Pake doublets. We assign the Pake doublet exhibiting the larger coupling constant of $q_{cc} = 4/3q_{zz} = 53$ kHz to the three fast rotating CD_3 groups of the σ-bonded C(NXyl)Cp* group whose Cp* ring is unable to rotate in the solid. The narrower Pake doublet (26 kHz) on the other hand is assigned to the η^5 bonded Cp* ring, subject to fast rotational 72° jumps. As temperature is decreased, the narrow component gradually disappears as the rate constants of the η^5 rotation become slow in the NMR time scale, until finally at 130 K almost all of the ^{2}H signal intensity of the η^5 bonded Cp* ring is broadened and superimposed on the Pake doublet of the nonrotating $C(NXyl)C_5Me_4CD_3$ unit.

An accurate line shape analysis of the ^{2}H NMR depicted in Figure 8 is difficult. However, a rough estimate of the rate

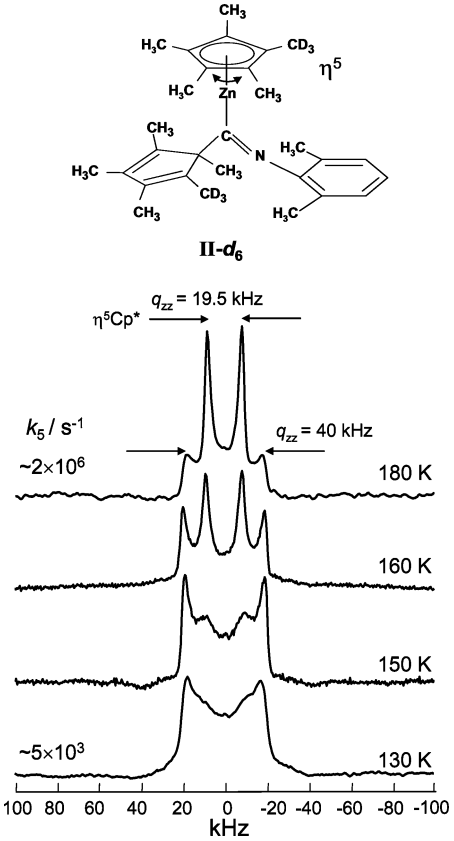

Figure 8. ^{2}H NMR spectra of compound **II**-d_6 measured with the solid echo technique and an echo delay of $\tau = 30$ μs.

constants k_5 of the 5-fold rotation of the η^5 bonded Cp* ring can be obtained by comparison of its line shape contribution with the calculated spectra of Figure S3 of Supporting Information. We obtain $k_5 \cong 2 \times 10^6$ sec^{-1} at 180 K and $k_5 \cong 5 \times 10^3$ sec^{-1} at 130 K. Considering an Arrhenius behavior for this motion and a preexponential factor log A/s^{-1} = 12.6, we obtain an activation energy for this process of $E_{a5} \cong 21$ kJ/mol.

Variable Temperature ^{2}H NMR of I-d_6. The superimposed experimental and calculated ^{2}H NMR spectra of **I**-d_6 recorded at different temperatures using the solid echo technique, and echo delays of $\tau = 30$ μs are shown in Figure 9. At 100 K, a single Pake doublet is observed for the two CD_3 groups of both rings, exhibiting a quadrupole coupling constant of $q_{cc} = 4q_{zz}/3 = 54$ kHz, where q_{zz} corresponds to the separation of the main peaks. As temperature is increased, the signal is gradually transformed into a reduced Pake doublet at 150 K, characterized by a motionally reduced quadrupolar coupling constant value of $q_{cc} = 23$ kHz. To account for the nonplanar methyl group conformation, the line shapes were simulated by considering 5-fold conical rotations, as explained in the Supporting Information (Figure S3).

Variable Temperature ^{2}H NMR Relaxation Times of Compound I-d_6. In this section, we describe the results of a study of the longitudinal ^{2}H NMR relaxation times of **I**-d_6. They were measured at 7 T using the saturation recovery technique. Within the margin of error, single-exponential magnetization built-up curves were observed at all temperatures. The data obtained are plotted as a function of the inverse temperature in Figure 10 and are listed in Table 2.

Three T_1 minima are observed at 220, 130, and 75 K. Each minimum corresponds to a different thermally activated kinetic process in the molecule that modulates the quadrupolar tensor and serves as a mechanism for the longitudinal relaxation. The

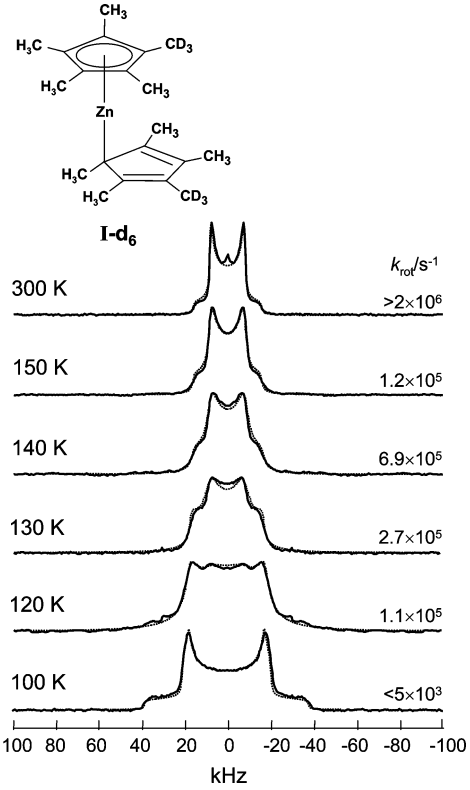

Figure 9. Variable temperature ^{2}H NMR spectra of compound **I**-d_6 recorded at 46.3 MHz with the solid echo sequence.

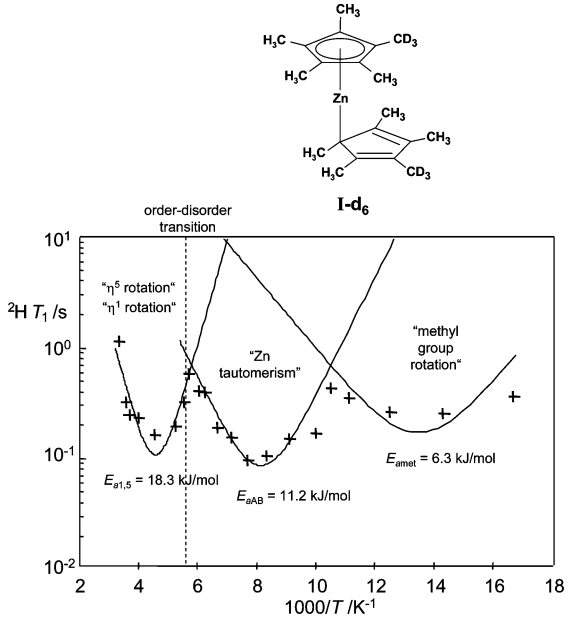

Figure 10. ^{2}H NMR longitudinal relaxation times of **I** measured at 7 T (46.3 MHz for ^{2}H) as a function of the inverse temperature. The fitting lines were calculated as described in the text.

rates of each relaxation mechanism can be described using the master equation for quadrupolar relaxation in the presence of exchange between two forms A and B[22]

$$\frac{1}{T_{1I}} = \frac{4CK_{AB}}{(K_{AB}+1)^2}\left(\frac{\tau}{1+\omega_I^2\tau^2} + \frac{4\tau}{1+4\omega_I^2\tau^2}\right) \qquad (10)$$

where K_{AB} is the equilibrium constant of the interconversion and τ the corresponding correlation time which can be expressed as

TABLE 2: ^{2}H Spin−Lattice Relaxation Times at Various Temperatures

T/K	^{2}H T_1/s	*T*/K	^{2}H T_1/s
300	1.16	140	0.15
280	0.33	130	0.10
270	0.25	120	0.12
250	0.24	110	0.15
220	0.16	100	0.17
190	0.19	95	0.44
180	0.25	90	0.35
175	0.80	80	0.26
165	0.41	70	0.34
160	0.40	60	0.46
150	0.16		

$$\tau^{-1} = k_{AB} + k_{BA} = A(\exp(-E_{aAB}/RT) + \exp(-(E_{aAB} - \Delta H)/RT)) \qquad (11)$$

Here, an Arrhenius law is used to describe the dependence of the forward and the backward rate constants on temperature.

For degenerate processes, eq 10 reduces to

$$\frac{1}{T_{1I}} = C\left(\frac{\tau}{1+\omega_I^2\tau^2} + \frac{4\tau}{1+4\omega_I^2\tau^2}\right) \qquad (12)$$

Usually, for intramolecular reactions, the pre-exponential factors are given by $A = 10^{12.6}$ s^{-1}. The solid lines in Figure 10 were calculated using eqs 10 to 12. The molecular processes giving rise to these data will be discussed in the next section.

Discussion

Using a combination of solid state ^{13}C and ^{2}H NMR, we have studied the molecular dynamics of polycrystalline ZnCp*$_2$ (**I**). Variable temperature high-resolution ^{13}C NMR experiments indicated a fast Zn tautomerism according to Figure 2a, which is degenerate above 210 K but becomes nondegenerate below this temperature. The degenerate Zn tautomerism above 210 K implies an interconversion of the η^5 and η^1 bound rings. Below this temperature, the two rings X and Y are inequivalent, where X exhibits a larger fraction of time in the η^5 state than Y. The ^{2}H NMR spectra of **I**-d_6 indicated slow Cp* ring dynamics around 100 K but fast dynamics at 150 K (Figure 9). By contrast, the spectra of **II**-d_6 revealed only a single fluxional Cp* ring. The longitudinal ^{2}H $-T_1$ relaxation times of **I**-d_6 exhibited three minima (Figure 10).

In this section, we will discuss all observations and develop a scenario of the fluxional behavior. In particular, we will discuss the motional model used to simulate the spectra of Figure 9.

Order−Disorder Transition of I and Thermodynamics of the Associated Zn Tautomerism. The variable-temperature ^{13}C CPMAS NMR spectra of **I** indicated only a single line for all carbons of the two Cp* rings down to 210 K. Below 210 K, however, a line splitting was observed which increased when temperature was further lowered (Figures 5 and 6). Such a behavior is typical for an order−disorder transition around 210 K, that is, the presence of a fast degenerate process at higher temperatures whose degeneracy is lifted at lower temperatures, as observed previously for the case of proton tautomerism in solids.[23] Because of fast 5-fold ring rotations discussed below, each ^{13}C line represents all carbon atoms of a given Cp* ring; hence, below 210 K, the two rings of **I** become inequivalent in the solid state. One line corresponds to a preferentially η^1-bound ring; the other corresponds to a preferentially η^5-bound ring. This behavior can be explained in terms of the Zn tautomerism between two forms A and B depicted in Figure 2; in the absence

of asymmetric isotope substitution, these two forms are related by a molecular inversion process. The equilibrium constants of this process could be measured by ^{13}C NMR, giving rise to a small reaction enthalpy of 2.4 kJ mol^{-1}. It follows that the η^1/η^5 mole fractions are different for both rings. However, as compared to the ^{13}C NMR time scale, the process is still fast down to 150 K where ^{13}C experiments could be performed.

We note that in previous ^{13}C CPMAS NMR studies on the related beryllocene,[12] a similar line splitting as shown in Figure 5 was observed which increased when the temperature was lowered. This finding was analyzed in terms of a molecular inversion process which is degenerate in the whole temperature regime but which presented a transition from fast to slow exchange. However, in the corresponding line shape analysis, temperature-dependent chemical shifts had to be assumed whose origin remained unexplained. Moreover, this analysis led to an unexpectedly high activation energy value of 36.9 kJ mol^{-1}, which was much larger than calculated values[11] which were of the order of 10 kJ mol^{-1}. It would be interesting to perform a similar analysis of the ^{13}C spectra of beryllocene as proposed here for decamethylzincocene, which would, however, require additional studies of model compounds in which the Be tautomerism is suppressed; there are good chances that beryllocene and decamethylzincocene behave in a similar way with respect to the order−disorder transition associated with the metal tautomerism.

Longitudinal Relaxation of I-d_6. In Figure 10, we assign the low-temperature minimum to the usual 3-fold methyl group rotational jumps depicted in Figure 2d. The high-temperature minimum occurs above the order−disorder transition and corresponds to the slowest process,that is, to averaged η^1/η^5 rotations of the Cp* rings (Figure 2b, 2c) which will be discussed in more detail in the next section. These processes are degenerate and were calculated using eq 12, using a simple Arrhenius law.

We assign the center minimum to the Zn tautomerism (Figure 2a), which is associated with the interconversion of the η^1 and η^5 bound rings. The solid center curve in Figure 10 was calculated using eqs 10 and 11, and the values of the reaction enthalpies and entropies obtained by ^{13}C NMR (eq 9). In all cases, the remaining parameters were then only the constants C in eqs 10 and 12, which are different for each process, and the corresponding forward activation energy. Both parameters were varied until the best agreement of the calculated curves with the experimental data was obtained. Thus, we obtained the energies of activation of $E_{a1,5} = 18.3$ kJ mol^{-1} for the averaged η^1/η^5 rotations, a forward energy of activation of $E_{aAB} = 11.2$ kJ mol^{-1} for the Zn tautomerism, and an energy of activation of $E_{a3} = 6.3$ kJ mol^{-1} for the methyl group rotation. The corresponding C factor in eq 10 used for the fittings was $C_3 = 2.4 \times 10^9$ s^{-2}.

The value of the energy of activation of the 3-fold methyl group rotation corresponds to what is expected for this kind of motions in the literature.[24] The activation energy of the Zn tautomerism is not much larger; at present, we are not aware of any reference value. However, we note that this value may be influenced by the intermolecular interactions in the crystal. The activation energy for the η^1/η^5 rotations in **I** of 18.3 kJ mol^{-1} is of the order expected for rotations of η^5 bound Cp* rings coordinated to transition metals η^5

Conclusions

We have demonstrated the presence of a number of superimposed fluxional processes according to Figure 2 in polycrystalline powdered samples of decamethylzincocene $ZnCp_2$* (**I**). Very important was the comparison with [(η^5-Cp*)Zn(C(NXyl)-C_5Me_5)] (**II**), where only a 5-fold rotation of the η^5 bound Cp* is possible. A second very important key was that both ^{13}C NMR experiments under CPMAS conditions and ^2H NMR of static powdered samples were measured. Only the combination of both methods allowed us to analyze the different processes in Figure 2, as ^{13}C NMR is sensitive to the Zn tautomerism and ^2H NMR to the ring rotations.

One important finding was that the Zn transition in solid **I** is degenerate above but nondegenerate below 210 K. This corresponds to a novel order−disorder phase transition. The origin of this ordering can be attributed to the influence of the electric dipole moment observed in this molecule[3a] due to its slip-sandwich disposition. Thus, one can expect a paraelectric disordered phase at high temperatures and an antiferroelectric or ferroelectric phase at low temperatures. It would be interesting in our opinion to further investigate this phenomenon and the nature of this phase transition.

The second important finding is the observation of similar activation energies for the 5-fold rotational jumps of the η^1 and the η^5 bound Cp* rings in **I**. This finding is in agreement with the structure **3** in Scheme 1, where both the η^5 and the η^1 rings exhibit π interactions with the metal. In contrast, one would expect for structure **4** in Scheme 1 a much slower rotation of the $\eta^1(\sigma)$ bond ring.

Acknowledgment. This research has been supported by the Deutsche Forschungsgemeinschaft, Bonn. We also thank the Fonds der Chemischen Industrie (Frankfurt), the Junta de Andalucía, and the Spanish Ministerio de Educación y Ciencia (MEC) (to E.C. Project CTQ2004-00409/BQU; FEDER support to R.F. for a Ramón y Cajal fellowship and for I.R. for a predoctoral fellowship).

Supporting Information Available: Introduction to the theory used for the ^2H NMR calculations, as well as model calculations in which the effects of the predicted tautomerisms of **I** in static ^2H NMR powder spectra as a function of rates and equilibrium constants are calculated. This material is available free of charge via the Internet at http://pubs.acs.org.

References and Notes

(1) (a) Togni, A.; Halterman, R. L.; *Metallocenes*, Vols. 1 and 2; Wiley: New York, 1998. (b) Scheirs, J.; Kaminsky, W.; *Metallocene-Based Polyolefins*, Vols. 1 and 2; John Wiley & Sons Ltd.: Chichester, 2000. (c) Togni, A.; Hayashi, T.; *Ferrocenes*; Verlag Chemie: Weinheim, 1995. (d) Jaouen, G.; Top, S.; Vessières, A.; Alberto, R. *J. Organomet. Chem.* **2000**, *600*, 23−36.

(2) (a) Kealy, T. J.; Pauson, P. L. *Nature* **1951**, *168*, 1039−1040. (b) Miller, S. A.; Tebboth, J. A.; Tremaine J. F. *J. Chem. Soc.* **1952**, 632−635.

(3) (a) Fischer, E. O.; Pfab, W. *Z. Naturforsh.* **1952**, *7b*, 377−379. (b) Wilkinson, G.; Rosenblum, M.; Whiting, M. C.; Woodward, R. B. *J. Am. Chem. Soc.* **1952**, *74*, 2125−2126. (c) Wilkinson, G. *J. Am. Chem. Soc.* **1952**, *74*, 6146−6149.

(4) (a) Fischer, E. O.; Hofman, H. P. *Chem. Ber.* **1959**, *92*, 482−486. (b) Fischer, E. O.; Hofmann, H. P.; Treiber, A. *Z. Naturforsh.* **1959**, *14b*, 599−608.

(5) (a) Jutzi, P.; Burford, N. *Chem. Rev.* **1999**, *99*, 969−990. (b) Janiak, C.; Schumann, H. *Adv. Organomet. Chem.* **1991**, *23*, 291. (c) Hays, M. L.; Hanusa, T. P. *Adv. Organomet. Chem.* **1996**, *40*, 117.

(6) (a) Hanusa, T. P. *Organometallics* **2002**, *21*, 2559−2571. (b) Jutzi, P.; Burford, N. *Metallocenes* Vol. 1; Togni, A., Haltermann, R. L., Eds.; Wiley: New York, 1998. (c) Jutzi, P. *J. Organomet. Chem.* **1990**, *400*, 1−17.

(7) Voigt, A.; Filipponi, S.; Macdonald, C. L. B.; Gorden, J. D.; Cowley, A. H. *Chem. Commun.* **2000.** 911−912.

(8) Fernández, R.; Resa, I.; del Río, D.; Carmona, E. *Organometallics* **2003**, *22*, 381−383.

(9) (a) Conejo, M. M.; Fernández, R.; Río, D.; Carmona, E.; Monge, A.; Ruiz, C.; Márquez, A. M.; Fernández Sanz, J. *Chem. Eur. J.* **2003**, *9*, 4452−4461. (b) Wong, C. J.; Lee, T. Y.; Cho, K. J.; Lee, S. *Acta Crystallogr. Sect. B* **1972**, *28*, 1662−1668. (c) Wong, C. H.; Lee, T. Y.; Lee, T. J.; Chang, T. W.; Liu, C. S. *Inorg. Nucl. Chem. Lett.* **1973**, *9*, 667−673. (d) Almenningen, A.; Haaland, A.; Lusztyk, J. *J. Organomet. Chem.* **1979**, *170*, 271−284. (e) Nugent, K. W.; Beattie, J. K.; Hambley, T. W.; Snow, M. R. *Aust. J. Chem.* **1984**, *37*, 35−45.

(10) (a) Burkey, D. J.; Hanusa, T. P. *J. Organomet. Chem.* **1996**, *512*, 165−173. (b) Fischer, B.; Wijkens, P.; Boersma, J.; van Koten, G.; Smeets, W. J. J.; Spek, L.; Budzelaar, P. H. M. *J. Organomet. Chem.* **1989**, *376*, 223−233. (c) Blom, R.; Boersma, J.; Budzelaar, P. H. M.; Fischer, B.; Haaland, A.; Volden, H. V.; Weidlein, J. *Acta Chem. Scand.* **1986**, *A40*, 113−120.

(11) (a) Margl, P.; Schwarz, K. *J. Am. Chem. Soc.* **1994**, *116*, 11177−11178. (b) Margl, P.; Schwarz, K. *J. Chem. Phys.* **1995**, *103*, 683−690.

(12) Hung, I.; Macdonald, C. L. B.; Schurko, R. W. *Chem. Eur. J.* **2004**, *10*, 5923−5935.

(13) (a) Alexander, S. *J. Chem. Phys.* **1962**, *37*, 971−977. (b) Binsch, G. *J. Am. Chem. Soc.* **1969**, *91*, 1304−1309. (c) Kleier, D. A.; Binsch, G. *J. Magn. Reson.* **1970**, *3*, 146−152.

(14) (a) Wehrle, B.; Zimmermann, H.; Limbach, H. H. *J. Am. Chem. Soc.* **1988**, *110*, 7014−7024. (b) Wehrle, B.; Limbach, H. H. *Chem. Phys.* **1989**, *136*, 223−247.

(15) Herrmann, W. A.; Salzer, A. In *Synthetic Methods of Organometallic and Inorganic Chemistry*; Herrmann, W. A., Ed.; Thieme: New York, 1996; Vol. 1, Chap. 3.

(16) (a) Wehrmann, F.; Albrecht, J.; Gedat, E.; Kubas, G. J.; Limbach, H. H.; Buntkowsky, G. *J. Phys. Chem. A* **2002**, *106*, 2855−2861. (b) Wehrmann, F.; Fong, T.; Morris, R. H.; Limbach, H. H.; Buntkowsky, G. *Phys. Chem. Chem. Phys.* **1999**, *1*, 4033−4041.

(17) Mehring, M. *High Resolution NMR Spectroscopy in Solids*; Springer-Verlag: New York, 1983.

(18) (a) Gedat, E.; Schreiber, A.; Albrecht, J.; Shenderovich, I.; Findenegg, G.; Limbach, H. H.; Buntkowsky, G. *J. Phys. Chem. B* **2002**, *106*, 1977. (b) Masierak, W.; Emmler, Th.; Gedat, E.; Schreiber, A.; Findenegg, G. H.; Buntkowsky, G. *J. Phys. Chem. B* **2004**, 18890−18896.

(19) Resa, I. Ph.D. Thesis, University of Sevilla, 2006.

(20) Conejo, M. M.; Fernández, R.; Carmona, E.; Andersen, R. A.; Gutierrez-Puebla, E.; Monge, M. A. *Chem. Eur. J.* **2003**, *9*, 4462−4471.

(21) Gutierrez-Puebla, E.; Monge, A., personal communication.

(22) Medycki, W. R.; Latanowicz, E. C. *Mol. Phys.* **1998**, *93*, 323−330.

(23) (a) Limbach, H. H. In *Encyclopedia of Nuclear Magnetic Resonance: Supplementary Volume 9, Advances in NMR;* Grant, D. M., Harris, R. K., Eds.; John Wiley & Sons, Ltd: Chichester, 2002; pp 520−531. (b) Foces-Foces, M. C.; Echevarría, A.; Jagerovic, N.; Alkorta, I.; Elguero, J.; Langer, U.; Klein, O.; Minguet-Bonvehí, M.; Limbach, H. H. *J. Am. Chem. Soc.* **2001**, *123*, 7898−7906.

(24) Del Rio, A.; Boucekkine, A.; Meinnel, J. *J. Comput. Chem.* **2003**, *24*, 2093−2100.